Supporting Information

Organic-inorganic haloargentate hybrids of [Me-dabco]Ag_2X_3 (X = I or Br) with halide ion manipulating crystal structure, phase transition and dielectric behavior

Xue-Wei Pan,[a] Qing-Qing Li,[a] Lu Zhai,*[a] Jin Zhang,[a] Wen-Long Liu,[b] Xiao-Ming Ren*[a,c]

[a] State Key Laboratory of Materials-Oriented Chemical Engineering and College of Chemistry and Molecular Engineering, Nanjing Tech University, Nanjing 211816, P. R. China

[b] College of Chemistry and Chemical Engineering, Yangzhou University, Yangzhou 225002, P. R. China

[c] State Key Laboratory of Coordination Chemistry, Nanjing University 210023, P. R. China

Tel: 86-25-58139476

E-mail: zhailu@njtech.edu.cn (LZ); xmren@njtech.edu.cn (XMR)

Table of Contents

C. Supporting Tables

D. References

A. Characterizations

Reagents and materials

All chemicals and reagents, including 1,4-diazabicyclob[2.2.2]octane (Dabco), $AgNO_3$, KI, KBr, methyl iodide, methyl bromide, N, N-dimethylformamide (DMF), acetone, methanol and ethanol were purchased from commercial suppliers and used as received.

General Methods

^{1}H-NMR spectra

^{1}H-NMR spectra of [Me-dabco]Br and [Me-dabco]I were recorded using a Bruker AVANCE III 400MHz NMR spectrometer. Both samples were prepared in DMSO-d6 solution form.

Single crystal structure

Single crystal structures of **1** and **2** were determined by Bruker SMART APEX-II diffractometer equipped with a CCD detector by Mo-Kα irradiation (wavelength equal to 0.71073 Å) at room temperature. The structure was analyzed by direct methods and refined with full-matrix least-square methods based on F^2 (SHELXL-2014 software package). All non-hydrogen atoms of the structure were refined anisotropically, hydrogen atoms were positioned geometrically and allowed to ride on their parent atoms with constrained thermal parameters. Crystal data and structure refinement parameters of **1** and **2** are summarized in Table S1. The CIF files of all structures can be found in the CCDC Database with deposition No. 2251761 and 2251765.

Powder X-ray diffraction (PXRD)

PXRD of polycrystalline powder was carried out by a MiniFlex600 X-ray diffractometer with Cu Kα (λ = 1.5404 Å) radiation in the 2-theat ranges of 5-50° with a step length of 0.02° to check the phase purity of the as-grown crystals, as given in Fig. S4.

IR and Raman spectra

The infrared (IR) and Raman measurements were measured to check the phases of the as-grown crystals. IR spectrum was recorded on a Thermo Scientific Nicolet iS10

spectrophotometer in the regime of 700–4000 cm^{-1}. Raman spectra was conducted on a Thermo Fisher Scientific DXR2 instrument with a 785 nm laser light irradiation from 57–3300 cm^{-1}. The results are presented in Fig. S5 and S6, with the characteristic peaks were identified as listed in Table S2.

TG and DSC

Thermogravimetric (TG) analysis was performed by TA2000 / 2960 analyzer in N_2 flow with a heating rate of 10 K/min in 307-800 K. Differential scanning calorimetry (DSC) measurement was taken by using a NETZSCH DSC 204F1 Phoenix calorimetry for powdered samples between –90 and 200 °C with a scan speed of 10 °C/min. As shown in Fig. S7, the two samples show similar three-step thermal decomposition behaviors, and thermal decomposition occurs at 553 and 529 K with significant mass loss percentage of 35.4 and 31.6 %, which corresponds to the release of the organic components [Me-dabco]X (X = I or Br) with the calculated mass loss of 35.1 and 35.5% for **1** and **2**, respectively.

Dielectrics

Alternating current (AC) conductivities, impedance spectra, and dielectric were measured under N_2 atmosphere using a Concept 80 system (Novocontrol, Germany) from –20 to 200 °C with the frequency of $1–10^7$ Hz. The powder sample was pressed into a pellet with a diameter of 7 mm. The pellet was layered between two parallel platinum electrodes.

B. Supporting Fig.s

(a)

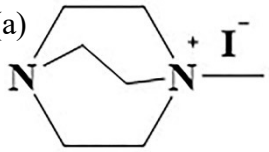

1-Methyl-1, 4-diazabicyclo[2.2.2]octan-1-ium Iodide

(b)

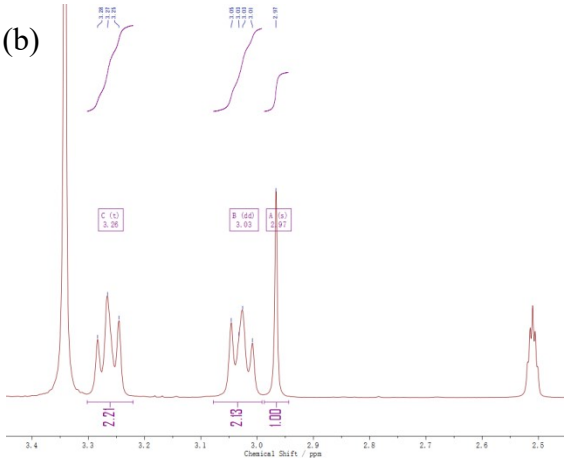

Fig. S1 (a) The chemical structure and (b) ^{1}H-NMR spectra of as-synthesized [Me-dabco]I (400 MHz, DMSO-d6): 2.96-2.98 (3 H, CH_3), 3.00-3.05 (6 H, 3 CH_2), 3.24-3.29 (6 H, 3 CH_2), 3.33-3.36 (H_2O), 2.50-2.52 (DMSO-d6).

(a)

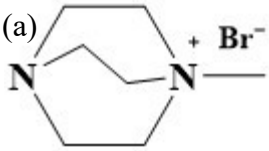

1-Methyl-1, 4-diazabicyclo[2.2.2]octan-1-ium bromide

(b)

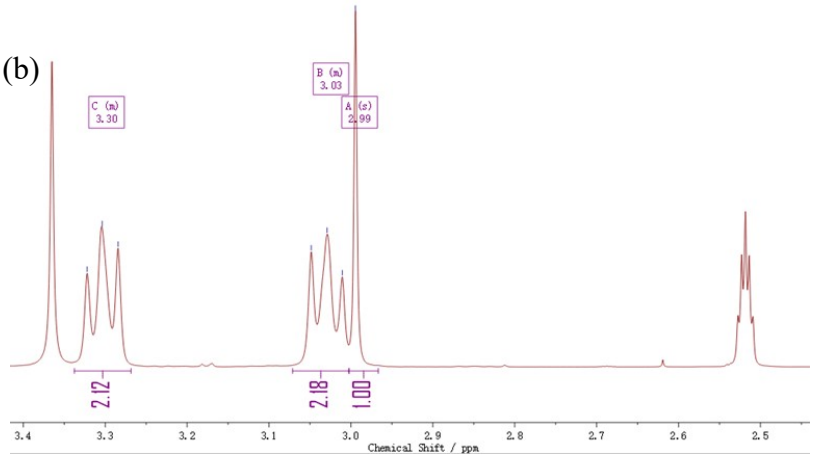

Fig. S2 (a) The chemical structure and (b) ^{1}H-NMR spectra of as-synthesized [Me-dabco]Br (400 MHz, DMSO-d6): 2.98-3.00 (3 H, CH_3), 3.00-3.06 (6 H, 3 CH_2), 3.28-3.33 (6 H, 3 CH_2), 3.35-3.37 (H_2O), 2.50-2.53 (DMSO-d6).

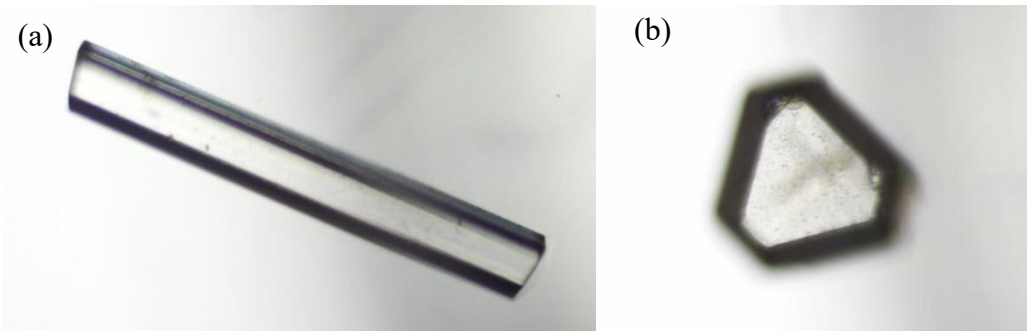

Fig. S3. Photographs of as-grown crystals of (a) **1** and (b) **2**.

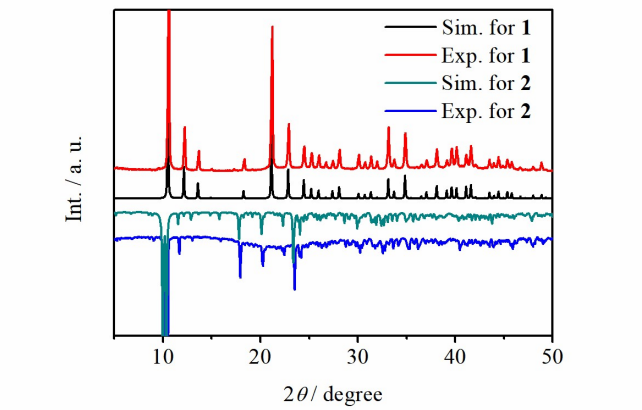

Fig. S4 The experimental PXRD patterns obtained at room temperature and simulated ones based on the single crystal structures of **1** and **2**.

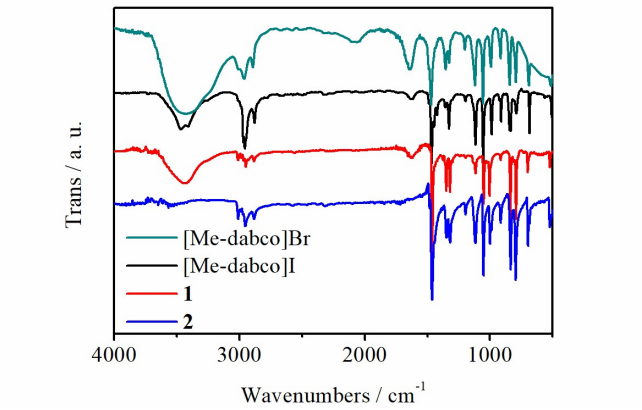

Fig. S5. FT-IR spectrum of **1** and **2** with [Me-dabco]X (X = I or Br).

Raman spectra of **1** and **2** are shown in Fig. S6. For **1**, the bands at 72 and

433–3014 cm^{-1} are assigned to the Raman active vibrations of [Me-dabco]I.[1] Compared with pure [Me-dabco]I, there are two new bands with Raman shifts of 90 and 110 cm^{-1} in the Raman spectra of **1** (Fig. S6), and these Raman active bands are attributed to the symmetrical stretching of Ag–I bonds and Ag lattice vibrational modes. It is worth noting that compared with pure AgI, the above two bands of **1** shift to higher wavenumbers, which may be related to the stronger bond energy of Ag-I bond. For **2**, The Raman spectrum is similar to that of pure [Me-dabco]Br except the band at 133 cm^{-1}. Given that AgBr has the characteristic peak at the same position, this peak may be attributed to the stretching vibrations between Ag^{+} and Br^{-} ions.[2]

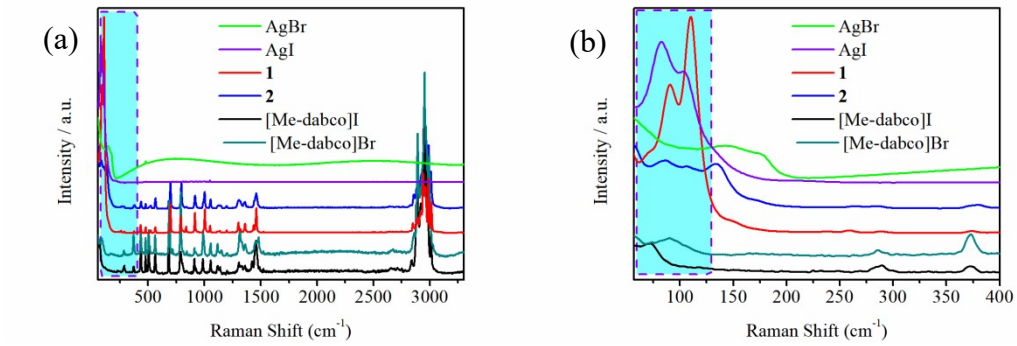

Fig. S6 Raman spectra of **1** and **2** with [Me-dabco]X (X = I or Br) obtained at different wavenumber range of (a) 57–3300 cm^{-1}, (b) 57–400 cm^{-1}.

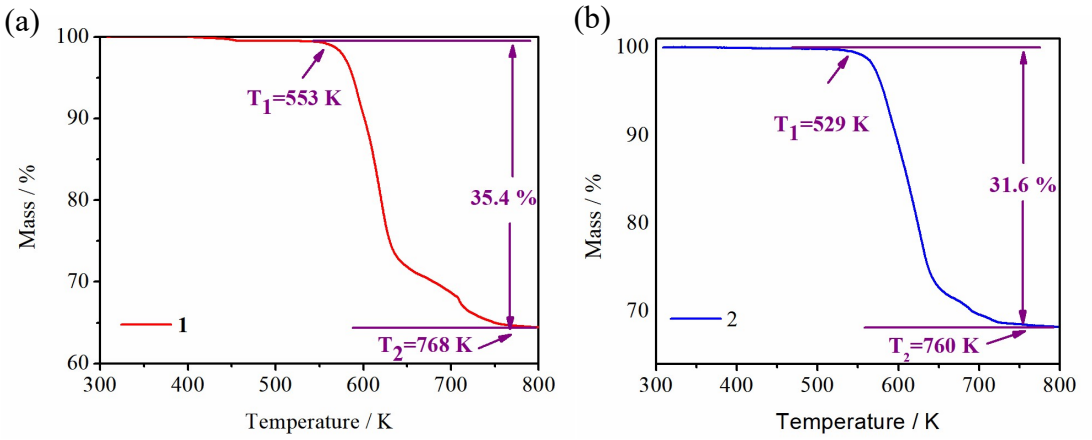

Fig. S7 TG curves of (a) **1** and (b) **2** in a N_2 atmosphere.

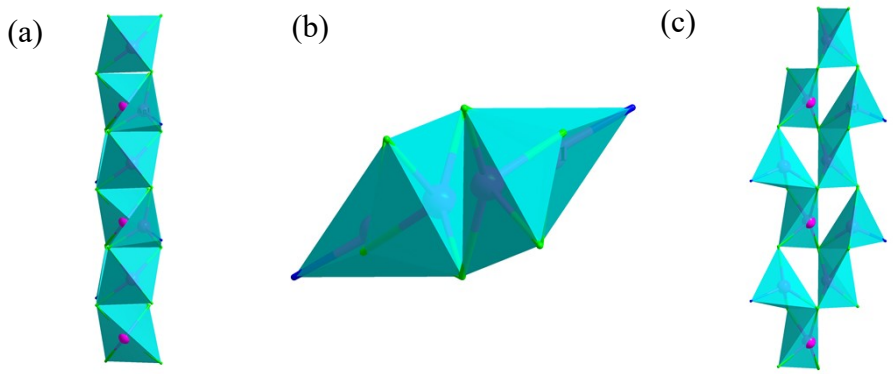

Fig. S8.Polyhedral view of the inorganic α-type neutral chain along (a) *a*-, (b) *b*- and (c) *c*-axis.

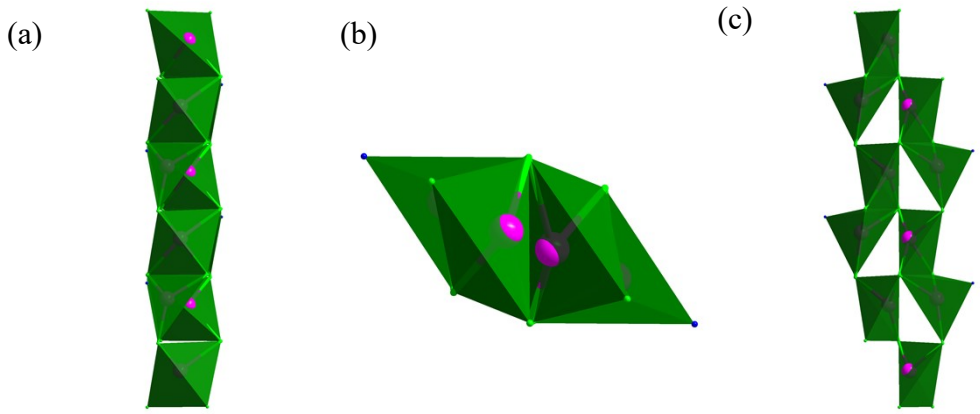

Fig. S9.Polyhedral view of the inorganic β-type neutral chain along (a) *a*-, (b) *b*- and (c) *c*-axis.

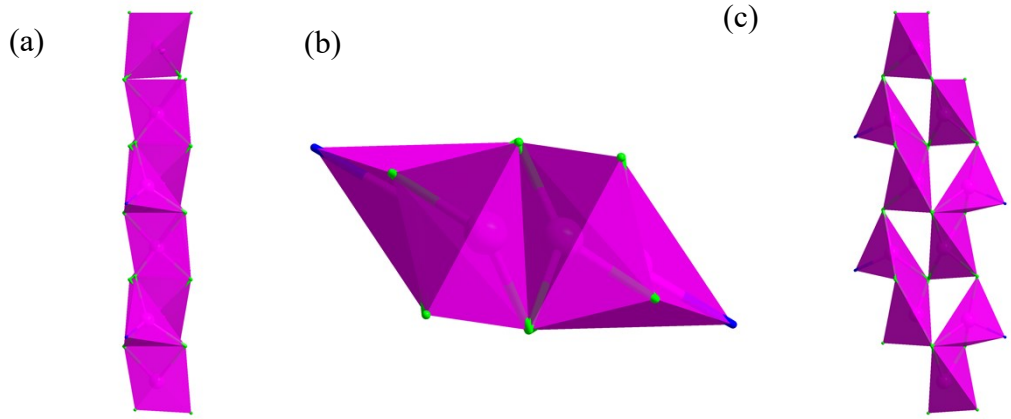

Fig. S10.Polyhedral view of the inorganic γ-type neutral chain along (a) *a*-, (b) *b*- and (c) *c*-axis.

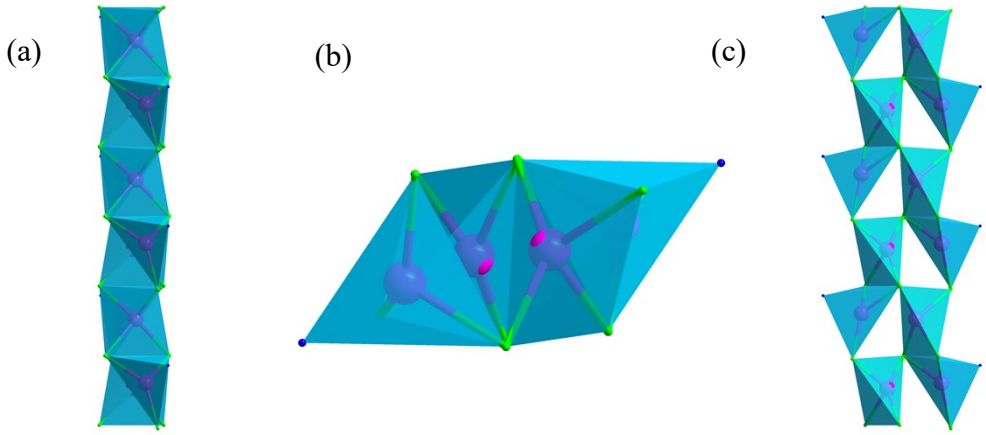

Fig. S11.Polyhedral view of the inorganic δ-type neutral chain along (a) *a*-, (b) *b*- and (c) *c*-axis.

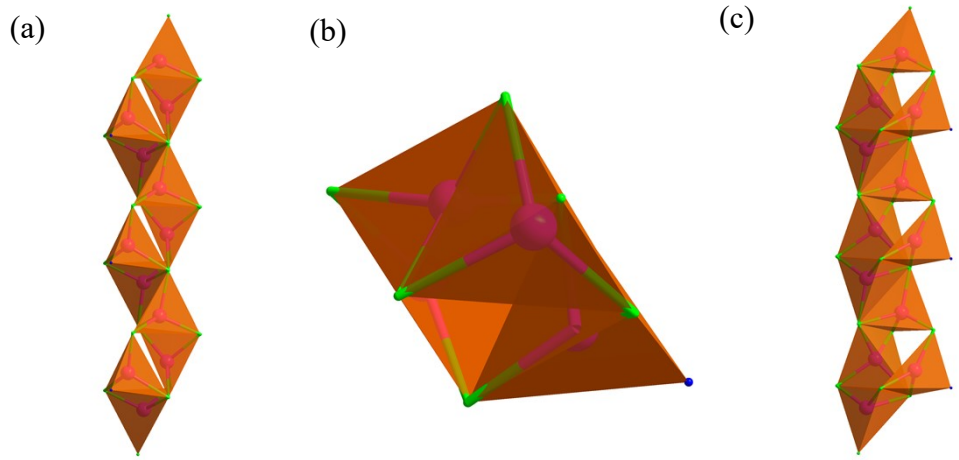

Fig. S12.Polyhedral view of the inorganic ε-type anionic chain along (a) *a*-, (b) *b*- and (c) *c*-axis.

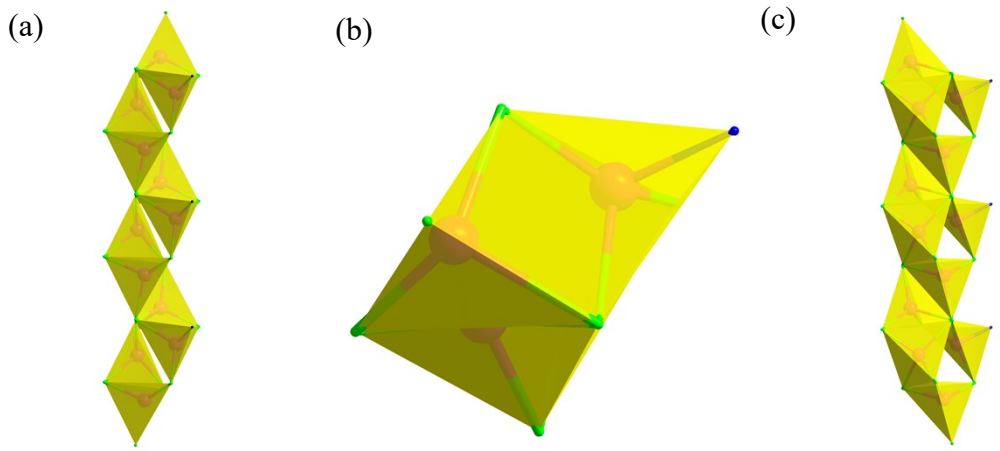

Fig. S13. Polyhedral view of the inorganic ζ-type anionic chain along (a) *a*-, (b) *b*- and (c) *c*-axis.

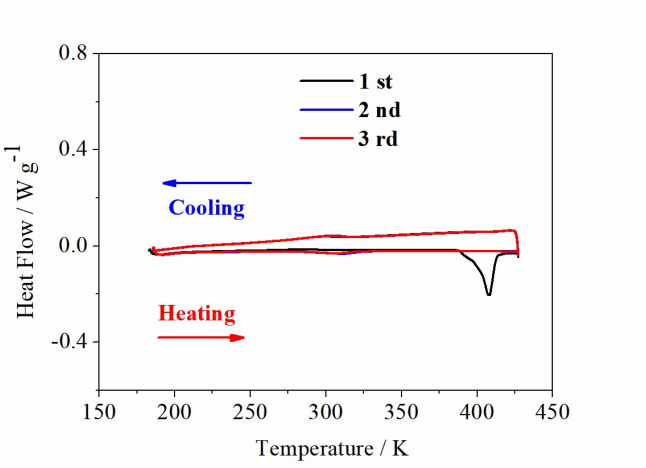

Fig. S14 The first three thermal cycles of **1** in the temperature range of 185–427 K.

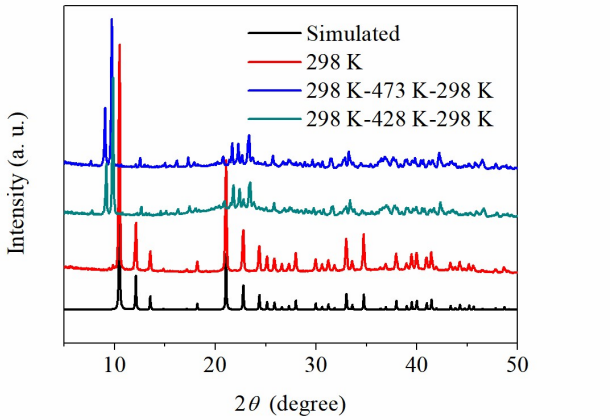

Fig. S15 Variable-temperature PXRD patterns of **1** within the 2θ range of 5-50°.

Since **2** crystallize in a noncentrosymmetric space group ($P2_1$), its second-harmonic generation (SHG) response was measured, using the Kurtz–Perry method with a home-built scanning microscope using an Nd:YAG laser (wavelength of 1064 nm, input pulse power of 400 mV) in reflection geometry. As displayed in Fig. S16a, **2** did exhibit SHG signal, even if very weak.

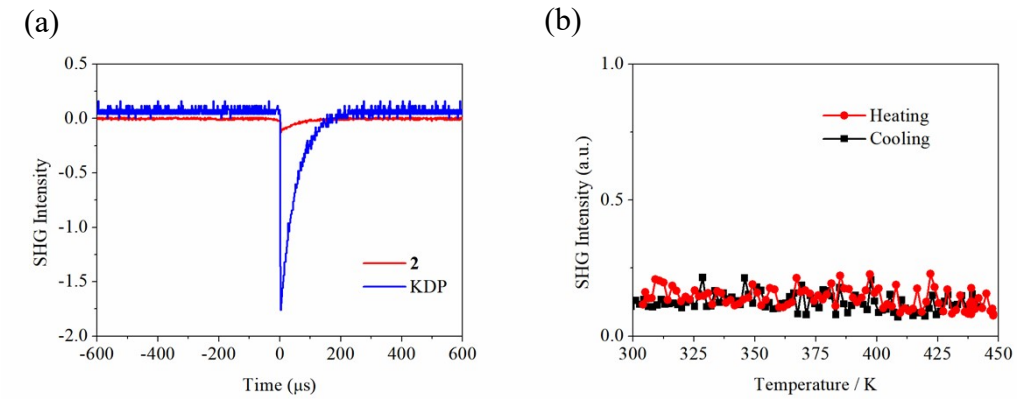

Fig. S16 (a) The comparison of SHG intensity between **2** and KDP at room temperature; (b) temperature-dependent SHG response of **2**.

C. Supporting Tables

Table S1 The crystallographic and structure refinement data for **1** and **2**

	1	**2**
Chemical formula	$C_7H_{15}N_2Ag_2I_3$	$C_7H_{15}N_2Ag_2Br_3$
CCDC number	2251761	2251765
Formula weight	723.65	582.65
Crystal system	Cubic	Monoclinic
Space group	*P*a-3	$P2_1$
a / Å	14.5961(3)	20.6830(17)
b / Å	14.5961(3)	7.4510(6)
c / Å	14.5961(3)	34.055(3)
α / °	90	90
β / °	90	90.169(3)
γ / °	90	90
V (Å^3) / Z	3109.64(19)/4	5248.1(8)/1
Calc.density g/cm^{-3}	3.091	2.950
Abs.coeff. μ/mms	8.448	12.088
F(000)	2592	4321
θ range for data collection /°	3.121 to 26.378	1.969 to 27.495
Index range	-16≤ h ≤18	-25≤ h ≤26
	-18≤ k ≤12	-9≤ k ≤9
	-17≤ l ≤18	-44≤ l ≤43
Refl. collected/unique	10993 / 1066	49598 / 22445
R_{int}	0.0712	0.0500
Goodness-of-fit on F^2	1.075	1.030
Final *R* indices [I>2σ(I)]	R_1 = 0.0323	R_1 = 0.0469
	wR_2 = 0.0655	wR_2 =0.0961
R indices(all data)	R_1 = 0.0419	R_1 = 0.0768

	wR_2 = 0.0710	wR_2 =0.1102
Residual(e Å $^{-3}$)	0.600/-0.623	1.192 / -1.109

$^{a}R_1=\sum||F_0|-|F_c|/\sum|F_0|$; $^{b}wR_2=\{\sum[w(F_0^2-F_c^2)^2]/\sum[w(F_0^2)^2]\}^{1/2}$

Table S2 The assignment of IR bands of **1** and **2**

1	**2**	assignments
3010s	3010s	ν_{as} (CH_3)
2984s	2987s	ν_{as} (CH_3)
2966s	2970s	ν_{as} (CH_3)
2949s	2952s	ν_{as} (CH_2)
2882s	2882s	ν_{s} (CH_3)
1460s	1461s	δ_{s} (CH_2) and δ_{as} (CH_3)
1349s	1345s	ν_{s} (NC_3)
1319s	1317s	ν(C-N)
1115s	1116s	ν(C-N)
1050s	1051s	ν(C-N) and ν_{as} (C-C)
1003s	1000s	δ(C-N)
837s	836s	$\delta(CH_2)_2$
792s	795s	$\delta(CH_2)_2$

Table S3 Bond lengths [Å] for **1** at 273 K

Atom pair	Distance / Å	Atom pair	Distance / Å
Ag(1)-Ag(1)$^{\#1}$	1.4299(14)	Ag(1)-Ag(1)$^{\#2}$	2.475(2)
Ag(1)-Ag(1)$^{\#3}$	1.4299(14)	Ag(1)-Ag(1)$^{\#4}$	2.475(2)
Ag(1)-Ag(1)$^{\#5}$	2.859(3)	Ag(1)-Ag(2)	2.944(9)
Ag(1)-I(1)$^{\#1}$	2.753(3)	Ag(1)-I(1)	2.790(3)
Ag(1)-Ag(2A)$^{\#5}$	2.874(8)	Ag(1)-Ag(2A)$^{\#2}$	2.839(8)
Ag(2)-I(1)$^{\#2}$	2.972(3)	Ag(2)-I(1)	2.972(3)
Ag(2)-I(1)$^{\#4}$	2.972(3)	Ag(2)-N(1)	2.442(13)
N(1)-Ag(2A)$^{\#4}$	2.432(10)	N(1)-Ag(2A)	2.432(10)
N(1)-Ag(2A)$^{\#2}$	2.432(10)	Ag(2A)-Ag(2A)$^{\#2}$	0.75(3)
Ag(2A)-Ag(2A)$^{\#4}$	0.75(3)		

Symmetry codes: #1 y,-z+1/2,x-1/2; #2 -y+1,z+1/2,-x+1/2; #3 z+1/2,x,-y+1/2;
#4 -z+1/2,-x+1,y-1/2; #5 -x+1,-y+1,-z

Table S4 Bond angles [°] for **1** at 273 K

Atoms	Angle / °	Atoms	Angle / °
Ag(1)$^{\#1}$-Ag(1)-Ag(1)$^{\#3}$	119.902(15)	Ag(1)$^{\#2}$-Ag(1)-Ag(1)$^{\#5}$	30.012(2)
Ag(1)$^{\#1}$-Ag(1)-Ag(1)$^{\#2}$	90.0	Ag(1)$^{\#4}$-Ag(1)-Ag(1)$^{\#5}$	30.012(2)
Ag(1)$^{\#3}$-Ag(1)-Ag(1)$^{\#4}$	90.0	Ag(1)$^{\#1}$-Ag(1)-Ag(1)$^{\#5}$	59.987(2)
Ag(1)$^{\#3}$-Ag(1)-Ag(1)$^{\#2}$	30.048(8)	Ag(1)$^{\#1}$-Ag(1)-Ag(1)$^{\#4}$	30.048(8)
Ag(1)$^{\#4}$-Ag(1)-Ag(1)$^{\#2}$	60.0	Ag(1)$^{\#3}$-Ag(1)-Ag(1)$^{\#5}$	59.987(2)
Ag(1)$^{\#5}$-Ag(1)-Ag(2)	61.85(12)	Ag(1)$^{\#4}$-Ag(1)-Ag(2)	65.14(9)
Ag(1)$^{\#3}$-Ag(1)-Ag(2)	77.56(13)	Ag(1)$^{\#2}$-Ag(1)-Ag(2)	65.14(9)
Ag(1)$^{\#1}$-Ag(1)-Ag(2)	77.57(13)	Ag(1)$^{\#1}$-Ag(1)-I(1)$^{\#1}$	76.50(15)
Ag(1)$^{\#3}$-Ag(1)-I(1)$^{\#1}$	127.7(2)	Ag(1)$^{\#2}$-Ag(1)-I(1)	92.16(16)
Ag(1)$^{\#2}$-Ag(1)-I(1)$^{\#1}$	127.75(4)	Ag(1)$^{\#3}$-Ag(1)-I(1)	73.62(14)
Ag(1)$^{\#4}$-Ag(1)-I(1)$^{\#1}$	97.15(15)	Ag(1)$^{\#1}$-Ag(1)-I(1)	134.3(2)
Ag(1)$^{\#4}$-Ag(1)-I(1)	127.16(5)	Ag(1)$^{\#2}$-Ag(1)-Ag(2A)$^{\#5}$	69.4(2)
Ag(1)$^{\#4}$-Ag(1)-Ag(2A)$^{\#5}$	73.7(4)	Ag(1)$^{\#2}$-Ag(1)-Ag(2A)$^{\#2}$	73.5(4)
Ag(1)$^{\#5}$-Ag(1)-Ag(2A)$^{\#5}$	67.7(3)	Ag(1)$^{\#1}$-Ag(1)-Ag(2A)$^{\#5}$	81.4(3)
Ag(1)$^{\#3}$-Ag(1)-Ag(2A)$^{\#5}$	74.2(2)	Ag(1)$^{\#4}$-Ag(1)-Ag(2A)$^{\#2}$	68.6(2)
Ag(1)$^{\#1}$-Ag(1)-Ag(2A)$^{\#2}$	76.9(2)	Ag(1)$^{\#3}$-Ag(1)-Ag(2A)$^{\#2}$	84.9(3)
I(1)$^{\#1}$-Ag(1)-Ag(1)$^{\#5}$	114.42(10)	I(1)-Ag(1)-Ag(1)$^{\#5}$	112.46(11)
I(1)$^{\#1}$-Ag(1)-Ag(2)	150.80(16)	I(1)-Ag(1)-Ag(2)	62.37(9)
I(1)$^{\#1}$-Ag(1)-I(1)	132.83(7)	I(1)-Ag(1)-Ag(2A)$^{\#2}$	60.3(2)
I(1)-Ag(1)-Ag(2A)$^{\#5}$	141.1(3)	I(1)$^{\#1}$-Ag(1)-Ag(2A)$^{\#2}$	145.5(3)
I(1)$^{\#1}$-Ag(1)-Ag(2A)$^{\#5}$	58.82(19)	Ag(2A)$^{\#2}$-Ag(1)-Ag(2A)$^{\#5}$	136.6(6)
Ag(2A)$^{\#2}$-Ag(1)-Ag(1)$^{\#5}$	68.9(3)	Ag(1)$^{\#2}$-Ag(2)-Ag(1)$^{\#1}$	57.7(2)
Ag(1)$^{\#4}$-Ag(2)-Ag(1)$^{\#1}$	27.91(9)	Ag(1)$^{\#5}$-Ag(2)-Ag(1)$^{\#1}$	49.03(17)
Ag(1)-Ag(2)-Ag(1)$^{\#1}$	27.91(9)	Ag(1)$^{\#2}$-Ag(2)-Ag(1)$^{\#3}$	27.91(9)
Ag(1)$^{\#4}$-Ag(2)-Ag(1)	49.72(17)	Ag(1)$^{\#2}$-Ag(2)-Ag(1)$^{\#4}$	49.72(17)
Ag(1)$^{\#4}$-Ag(2)-Ag(1)$^{\#3}$	57.7(2)	Ag(1)$^{\#2}$-Ag(2)-Ag(1)$^{\#5}$	27.91(9)
Ag(1)-Ag(2)-Ag(1)$^{\#3}$	27.91(9)	Ag(1)$^{\#5}$-Ag(2)-Ag(1)$^{\#3}$	49.03(17)
Ag(1)$^{\#2}$-Ag(2)-Ag(1)	49.72(17)	Ag(1)-Ag(2)-Ag(1)$^{\#5}$	57.7(2)
Ag(1)$^{\#3}$-Ag(2)-Ag(1)$^{\#1}$	49.03(17)	Ag(1)-Ag(2)-I(1)$^{\#4}$	79.9(2)
Ag(1)$^{\#4}$-Ag(2)-Ag(1)$^{\#5}$	27.91(9)	Ag(1)-Ag(2)-I(1)	56.28(13)
Ag(1)$^{\#2}$-Ag(2)-I(1)$^{\#2}$	56.28(13)	Ag(1)$^{\#4}$-Ag(2)-I(1)	105.8(3)
Ag(1)-Ag(2)-I(1)$^{\#2}$	105.8(3)	Ag(1)$^{\#2}$-Ag(2)-I(1)$^{\#4}$	105.8(3)
Ag(1)$^{\#4}$-Ag(2)-I(1)$^{\#4}$	56.28(13)	Ag(1)$^{\#2}$-Ag(2)-I(1)	79.9(2)
Ag(1)$^{\#4}$-Ag(2)-I(1)$^{\#2}$	79.9(2)	I(1)-Ag(2)-Ag(1)$^{\#3}$	55.07(12)
I(1)$^{\#4}$-Ag(2)-Ag(1)$^{\#5}$	82.5(2)	I(1)$^{\#2}$-Ag(2)-Ag(1)$^{\#5}$	55.07(12)
I(1)-Ag(2)-Ag(1)$^{\#5}$	104.1(3)	I(1)$^{\#4}$-Ag(2)-Ag(1)$^{\#1}$	55.07(12)
I(1)-Ag(2)-Ag(1)$^{\#1}$	82.5(2)	I(1)$^{\#2}$-Ag(2)-Ag(1)$^{\#1}$	104.1(3)
I(1)$^{\#2}$-Ag(2)-Ag(1)$^{\#3}$	82.5(2)	I(1)$^{\#2}$-Ag(2)-I(1)$^{\#4}$	117.01(12)
I(1)$^{\#4}$-Ag(2)-Ag(1)$^{\#3}$	104.1(3)	I(1)$^{\#2}$-Ag(2)-I(1)	117.01(12)
I(1)$^{\#4}$-Ag(2)-I(1)	117.01(12)	N(1)-Ag(2)-Ag(1)	150.96(10)
N(1)-Ag(2)-Ag(1)$^{\#1}$	151.37(10)	N(1)-Ag(2)-Ag(1)$^{\#2}$	150.96(10)

N(1)-Ag(2)-Ag(1)$^{\#4}$	150.96(10)	N(1)-Ag(2)-Ag(1)$^{\#3}$	151.37(10)
N(1)-Ag(2)-Ag(1)$^{\#5}$	151.37(10)	N(1)-Ag(2)-I(1)$^{\#4}$	100.1(2)
N(1)-Ag(2)-I(1)$^{\#2}$	100.1(2)	Ag(1)$^{\#3}$-I(1)-Ag(1)	29.89(5)
N(1)-Ag(2)-I(1)	100.1(2)	Ag(1)-I(1)-Ag(2)	61.3(2)
Ag(1)$^{\#3}$-I(1)-Ag(2)	62.7(2)	C(1)-N(1)-Ag(2)	110.3(3)
C(1)$^{\#4}$-N(1)-Ag(2)	110.3(3)	C(1)-N(1)-Ag(2A)#4	100.9(5)
C(1)$^{\#2}$-N(1)-Ag(2)	110.3(3)	C(1)$^{\#2}$-N(1)-Ag(2A)	100.9(5)
C(1)$^{\#2}$-N(1)-Ag(2A)$^{\#4}$	118.3(5)	C(1)-N(1)-Ag(2A)$^{\#2}$	118.3(5)
C(1)$^{\#4}$-N(1)-Ag(2A)$^{\#4}$	111.2(4)	C(1)$^{\#2}$-N(1)-Ag(2A)$^{\#2}$	111.2(4)
C(1)$^{\#4}$-N(1)-Ag(2A)	118.3(5)	C(1)$^{\#4}$-N(1)-Ag(2A)$^{\#2}$	100.9(5)
C(1)-N(1)-Ag(2A)	111.2(4)	Ag(2A)-N(1)-Ag(2A)$^{\#4}$	17.7(7)
Ag(2A)-N(1)-Ag(2A)$^{\#2}$	17.7(7)	Ag(1)$^{\#5}$-Ag(2A)-Ag(1)$^{\#1}$	49.16(13)
Ag(2A)$^{\#2}$-N(1)-Ag(2A)$^{\#4}$	17.7(7)	Ag(1)$^{\#2}$-Ag(2A)-Ag(1)	46.92(17)
Ag(1)$^{\#1}$-Ag(2A)-Ag(1)	26.32(10)	Ag(1)$^{\#5}$-Ag(2A)-Ag(1)$^{\#3}$	47.48(16)
Ag(1)$^{\#4}$-Ag(2A)-Ag(1)$^{\#3}$	55.83(17)	Ag(1)$^{\#4}$-Ag(2A)-Ag(1)$^{\#2}$	49.96(13)
Ag(1)$^{\#1}$-Ag(2A)-Ag(1)$^{\#3}$	46.29(16)	Ag(1)$^{\#5}$-Ag(2A)-Ag(1)$^{\#2}$	28.00(8)
Ag(1)$^{\#2}$-Ag(2A)-Ag(1)$^{\#1}$	56.14(16)	Ag(1)$^{\#4}$-Ag(2A)-Ag(1)$^{\#1}$	27.71(8)
Ag(1)$^{\#2}$-Ag(2A)-Ag(1)$^{\#3}$	26.23(10)	Ag(1)$^{\#4}$-Ag(2A)-Ag(1)$^{\#5}$	28.98(8)
Ag(1)$^{\#4}$-Ag(2A)-Ag(1)	48.02(16)	Ag(1)$^{\#5}$-Ag(2A)-Ag(1)	55.93(17)
Ag(1)-Ag(2A)-Ag(1)$^{\#3}$	25.75(10)	N(1)-Ag(2A)-Ag(1)$^{\#1}$	146.0(5)
N(1)-Ag(2A)-Ag(1)$^{\#4}$	163.4(5)	N(1)-Ag(2A)-Ag(1)	135.6(6)
N(1)-Ag(2A)-Ag(1)$^{\#2}$	146.5(5)	N(1)-Ag(2A)-Ag(1)$^{\#3}$	136.4(7)
N(1)-Ag(2A)-Ag(1)$^{\#5}$	164.7(4)	Ag(2A)$^{\#4}$-Ag(2A)-Ag(1)$^{\#3}$	56.0(2)
Ag(2A)$^{\#4}$-Ag(2A)-Ag(1)$^{\#2}$	69.6(6)	Ag(2A)$^{\#4}$-Ag(2A)-Ag(1)$^{\#4}$	111.8(3)
Ag(2A)$^{\#4}$-Ag(2A)-Ag(1)$^{\#5}$	97.6(6)	Ag(2A)$^{\#2}$-Ag(2A)-Ag(1)$^{\#3}$	71.0(5)
Ag(2A)$^{\#2}$-Ag(2A)-Ag(1)$^{\#2}$	97.2(6)	Ag(2A)$^{\#2}$-Ag(2A)-Ag(1)$^{\#5}$	111.5(3)
Ag(2A)$^{\#2}$-Ag(2A)-Ag(1)	55.6(2)	Ag(2A)$^{\#4}$-Ag(2A)-Ag(1)	69.3(5)
Ag(2A)$^{\#2}$-Ag(2A)-Ag(1)$^{\#4}$	96.1(6)	Ag(2A)$^{\#2}$-Ag(2A)-N(1)	81.2(4)
Ag(2A)$^{\#4}$-Ag(2A)-N(1)	81.2(4)	Ag(2A)$^{\#2}$-Ag(2A)-Ag(2A)$^{\#4}$	59.997(5)

Symmetry codes: #1 y,-z+1/2,x-1/2; #2 -y+1,z+1/2,-x+1/2; #3 z+1/2,x,-y+1/2; #4 -z+1/2,-x+1,y-1/2; #5 -x+1,-y+1,-z

Table S5 Bond lengths [Å] for **2** at 273 K

Atom pair	Distance / Å	Atom pair	Distance / Å
Ag(1)-Ag(2)$^{\#1}$	2.9811(19)	Ag(1)-Br(1)	2.5774(19)
Ag(1)-Br(2)	2.7423(19)	Ag(1)-Br(3)	2.666(2)
Ag(1)-N(1)	2.499(13)	Ag(2)-Br(1)	2.746(2)
Ag(2)-Br(2)$^{\#2}$	2.819(2)	Ag(2)-Br(2)$^{\#3}$	2.912(2)
Ag(2)-Br(3)$^{\#2}$	2.860(2)	Ag(3)-Ag(4)$^{\#4}$	2.9761(16)
Ag(3)-Br(4)	2.5805(19)	Ag(3)-Br(5)	2.666(2)
Ag(3)-Br(6)	2.746(2)	Ag(3)-N(5)	2.491(11)
Ag(4)-Br(4)	2.7384(19)	Ag(4)-Br(5)$^{\#5}$	2.867(2)
Ag(4)-Br(6)$^{\#6}$	2.912(2)	Ag(4)-Br(6)$^{\#5}$	2.822(2)
Ag(5)-Ag(6)$^{\#7}$	2.9980(17)	Ag(5)-Br(7)	2.628(2)
Ag(5)-Br(8)	2.5801(19)	Ag(5)-Br(9)$^{\#5}$	2.817(2)
Ag(5)-N(6)	2.534(10)	Ag(6)-Br(7)$^{\#2}$	2.816(2)
Ag(6)-Br(8)	2.7281(18)	Ag(6)-Br(9)$^{\#7}$	2.7650(18)
Ag(6)-Br(9)	2.750(2)	Ag(7)-Ag(8)	3.2846(18)
Ag(7)-Br(12)	2.609(2)	Ag(7)-Br(13)	2.586(2)
Ag(7)-Br(15)$^{\#5}$	2.800(2)	Ag(7)-N(8)	2.516(11)
Ag(8)-Ag(9)	3.164(2)	Ag(8)-Ag(10)	3.099(2)
Ag(8)-Br(10)$^{\#2}$	2.810(2)	Ag(8)-Br(11)	2.703(2)
Ag(8)-Br(14)	2.714(2)	Ag(8)-Br(15)$^{\#5}$	2.908(2)
Ag(9)-Ag(10)$^{\#5}$	2.970(2)	Ag(9)-Br(10)	2.687(2)
Ag(9)-Br(11)	2.649(2)	Ag(9)-Br(12)	2.664(2)
Ag(9)-Br(15)$^{\#5}$	3.000(2)	Ag(10)-Br(10)$^{\#2}$	2.859(2)
Ag(10)-Br(13)	2.6286(19)	Ag(10)-Br(14)	2.674(2)
Ag(10)-Br(15)	2.770(2)	Ag(11)-Ag(13)	3.293(2)
Ag(11)-Br(18)	2.6015(19)	Ag(11)-Br(19)	2.585(2)
Ag(11)-Br(20)$^{\#2}$	2.801(2)	Ag(11)-N(11)	2.518(12)
Ag(12)-Ag(13)	3.161(2)	Ag(12)-Ag(14)$^{\#2}$	2.964(2)
Ag(12)-Br(16)	2.658(2)	Ag(12)-Br(18)	2.672(3)
Ag(12)-Br(20)$^{\#2}$	2.9898(19)	Ag(12)-Br(21)	2.683(2)
Ag(13)-Ag(14)	3.101(2)	Ag(13)-Br(16)	2.704(2)
Ag(13)-Br(17)	2.710(2)	Ag(13)-Br(20)$^{\#2}$	2.905(2)
Ag(13)-Br(21)$^{\#5}$	2.807(2)	Ag(14)-Br(17)	2.675(2)
Ag(14)-Br(19)	2.638(2)	Ag(14)-Br(20)	2.772(2)
Ag(14)-Br(21)$^{\#5}$	2.851(2)	Ag(15)-Ag(16)$^{\#8}$	3.0029(19)
Ag(15)-Br(22)	2.5810(19)	Ag(15)-Br(23)$^{\#2}$	2.8146(17)
Ag(15)-Br(24)	2.630(2)	Ag(15)-N(12)	2.564(12)
Ag(16)-Br(22)	2.734(2)	Ag(16)-Br(23)	2.7480(19)
Ag(16)-Br(23)$^{\#8}$	2.769(2)	Ag(16)-Br(24)$^{\#5}$	2.811(2)

Symmetry codes: #1 -x+1,y-1/2,-z+2; #2 x,y+1,z; #3 -x+1,y+1/2,-z+2; #4 -x,y+1/2,-z+1; #5 x,y-1,z; #6 -x,y-1/2,-z+1; #7 -x+1,y-1/2,-z+1; #8 -x+2,y+1/2,-z; #9 -x+1,y+1/2,-z+1; #10 -x+2,y-1/2,-z

D. References

1. V. I. Kovalenko, A. A. Akhmadiyarov, A. E. Vandyukov, A. R. Khamatgalimov, J. *Mol. Struct*. 2012, **1028**, 134–140.
2. J. X. Yu, M. Cui, X. Z. Liu, Q. Q. Chen, Y. Wu, Y. M. He, *Mater. Lett*, 2017, **193**, 73–76.